A Synergistic Hybrid CPCM–Liquid Thermal Management System for High-Power Battery Modules

Temesgen Abera Takiso , Jianwu Yu * , Girum Girma Bizuneh

Posted Date: 18 May 2026

doi: 10.20944/preprints202605.1153.v1

Keywords: lithium-ion battery; thermal management system; composite phase change material; leaf-shaped cold plate; flow channel topology

 doi:10.20944/preprints202605.1153.v1

Article

A Synergistic Hybrid CPCM–Liquid Thermal Management System for High-Power Battery Modules

Temesgen Abera Takiso [1], Jianwu Yu [1,*] and Girum Girma Bizuneh [2]

[1] College of Mechanical and Vehicle Engineering, Hunan University, Changsha, Hunan, China

[2] School of Physics and Electronics, Hunan University, Changsha, Hunan, China

* Correspondence: yokenbu@hnu.edu.cn; Tel.: +8615874162195

Abstract

Rising demand for high-performance battery thermal management systems (BTMS) has rendered single-mode cooling insufficient for advanced lithium-ion batteries (LIBs) in new energy vehicles (NEVs), particularly under high discharge rates. This study proposes a synergistic hybrid BTMS integrating composite phase change material (CPCM)–Aluminum foam with liquid cooling to enhance thermal regulation of cylindrical battery modules under 5 C discharge conditions. Multiple liquid cooled plate (LCP) configurations, including serpentine, straight, and leaf-shaped designs, together with different flow channel topologies (FCTs), were systematically investigated and optimized. The effects of coolant flow speed (CFS) and ambient temperature are also analyzed. Results indicate that the optimized leaf-shaped LCP with FCT #2 delivers superior performance, limiting the maximum temperature to 309.98 K, reducing temperature difference by 7.6 %, and decreasing pressure drop by 88.79 % compared to the serpentine configuration. Increasing CFS improves heat dissipation and delays PCM melting, although it raises pressure losses. Furthermore, the proposed system maintains a cell-to-cell temperature difference below 0.51 K, indicating excellent thermal uniformity. Compared to a CPCM-only system, the hybrid BTMS reduces peak temperature by 8.81 K under elevated ambient conditions (309.15 K), demonstrating strong potential for reliable and efficient thermal management in demanding operating environments.

Keywords: lithium-ion battery; thermal management system; composite phase change material; leaf-shaped cold plate; flow channel topology

1. Introduction

The urgent transition of the transportation sector away from reliance on conventional petroleum-based energy toward resilient and sustainable alternatives is essential for mitigating global warming and achieving the net-zero CO_2 emissions goal by 2050 [1]. In this context, LIBs have emerged as a dominant energy storage pathway for NEVs due to their high energy density, long cycle life, and absence of memory effects [2]. Despite these advantages, the performance, lifespan, and safety of LIBs are highly sensitive to their operating temperature (OT). Exposure to elevated temperatures accelerates battery degradation, reduces capacity, and increases the risk of critical safety issues, including thermal runaway (TR) [3]. Therefore, effective thermal regulation is crucial to enhance power output, safety, and reliable battery operation. Maintaining an optimal OT range is particularly important; typically, LIBs should operate between 20 °C and 40 °C, while the temperature variation within a battery module should not exceed 5 °C to ensure thermal uniformity and prevent localized overheating [4].

Consequently, the BTMS is a critical component in electric vehicles and other energy storage systems, responsible for maintaining safe operating temperatures, ensuring system safety, and extending battery lifespan. Among the various BTMS approaches, air-based, liquid-based, PCM-

 doi:10.20944/preprints202605.1153.v1

based, and hybrid systems (combination) are widely adopted and have demonstrated effectiveness in temperature regulation within battery modules [5]. Air-based BTMSs are particularly attractive due to their simplicity, low cost, and ease of implementation; however, their performance is limited by the low thermal conductivity of air, especially under high heat generation or demanding operating conditions. Thus, their effectiveness in advanced applications remains hindered.

To overcome the aforementioned limitations, performance improvements have been pursued via optimization of airflow distribution, including refined channel designs and enhanced inlet–outlet configurations [6,7]. Such design modifications increase heat transfer (HT) and promote evenly distributed temperature within the battery system. Xiaoming et al. [8] experimentally investigated how different duct shapes enhance flow paths to improve the TMP of forced air BTMS under various operating conditions. Their results showed that a double U-shaped air-cooling duct offers better cooling performance than a double I-shaped duct, maintaining the temperature difference across the entire battery module below 3 °C. Besides, to enhance air-based BTMS performance, Chen et al. [9] designed airflow patterns with different inlet and outlet regions. Placing the outlet at the midpoint of the convergence plenum lowered the maximum battery temperature by 4.5 K and the maximum temperature variation by 7.7 K relative to a typical Z-shaped system. Furthermore, by replacing straight walls with wavy channel walls in an air-cooled BTMS, Singh et al. [10] reduced the maximum battery temperature by 10 K compared to traditional designs.

Liquid-based BTMSs represent a commercially attractive option, particularly for large-scale battery packs. Thanks to their superior heat dissipation, high cooling efficiency, and compact architecture, they are well-suited for high-capacity energy storage systems [11]. Extensive research has been conducted to improve the TMP of liquid-based BTMSs. For 18,650-type LIB cells, Mitra et al. [12] designed a novel liquid-based BTMS featuring single or double serpentine channels under different flow configurations. Among these, the dual serpentine channel with counterflow configuration proved most effective, lowering the maximum battery temperature by approximately 13 °C and the module's temperature variation by approximately 3 °C. Lai et al. [13] proposed a lightweight liquid BTMS for 18650-type LIBs under a 5 C discharge rate. The system significantly improved cooling performance, limiting the maximum temperature below 313 K and reducing temperature variation by 14 %. The integration of metal fins into cooling systems enhances HT. Guo et al. [14] developed a mini-channeled LCP with circular pin fins to improve LIB cooling performance. Their results showed that horizontally arranged pin fins provided superior cooling compared to vertical arrangements and pin-free designs.

PCM-based BTMS has emerged as a promising cooling approach, mainly because it operates passively, storing thermal energy in the form of latent heat without consuming extra pumping energy. PCM-based BTMS effectively reduces the OT of LIBs, thereby controlling the battery within a recommended temperature threshold and reducing the risk of TR. Bernardo et al. [15] demonstrated that a PCM-based BTMS can significantly delay the rise in LIB temperature from reaching its critical levels until the paraffin RT-42 is fully melted. Kumar et al. [16] conducted a comparative study of PCM- and air-based BTMS. The results showed that, with PCM cooling, the battery required 350 % longer to reach 60 °C compared to natural air cooling. Furthermore, thermal performance was enhanced by incorporating fins, with the battery operating time increasing by 21 % when eight fins were integrated into the PCM system. Nevertheless, its real-world application is constrained by limited thermal conductivity and leakage issues, which hinder HT efficiency and prolonged reliability [17].

Hybrid-based BTMSs, another combine approaches, demonstrated notable potential in improving TMP, making them particularly favorable for thermal regulation in high-power LIB applications. Their performance efficiency arises from the integration of passive and active cooling techniques, which offer enhanced HT compared to conventional single-mode approaches [5,18,19]. By combining the advantages of passive thermal storage and active heat dissipation, hybrid BTMSs can achieve superior TMP, particularly under demanding operating conditions. For instance, Ammar et al. [20] conducted a comparative study of three thermal management approaches, namely PCM-

 doi:10.20944/preprints202605.1153.v1

based, liquid cooling, and hybrid BTMS. The results indicated that the hybrid approach exhibited superior TMP compared to the others, reducing the maximum temperature and temperature non-uniformity by 5.30 °C and 0.80 °C, respectively. Similarly, Wu et al. [21] proposed a hybrid system (combining a PCM, a heat pipe, and a thermoelectric cooler) that achieves a superior TMP compared to other single-mode cooling strategies, while maintaining the maximum temperature and temperature non-uniformity below 299.20 K and 3.46 K, respectively. Rahmani et al. [22] performed numerical studies on a BTMS combining air-based, LCP, and porous media under a 5 C discharge rate. The findings indicate that this hybrid configuration significantly enhances thermal regulation, thereby improving battery performance, safety, and cycle life.

Among various hybrid approaches, PCM–liquid-based BTMS have gotten researchers' attention worldwide due to their potential to absorb large amounts of heat through latent heat storage while simultaneously facilitating continuous heat removal through liquid (active) cooling strategies. Rabiei et al. [23] investigated a hybrid BTMS incorporating a microchannel LCP combined with PCM under a 5 C discharge rate. The results showed that the maximum temperature and temperature non-uniformity were reduced by 2.43 °C and 5.22 °C, respectively. In subsequent studies, Chen et al. [24] proposed an LCP with forked channels integrated with PCM to enhance uniform fluid flow distribution. This design demonstrated a significant improvement in TMP, achieving a maximum battery module temperature of 308.70 K and a temperature non-uniformity of 2.90 K under a 4C-rate. Hyun et al. [25] developed a hybrid BTMS that integrates PCM-LCP with various channel configurations. The study concluded that this hybrid BTMS improves TMP, reducing battery temperature by 17.80 % and demonstrating its effectiveness in maintaining LIBs within optimal OT limits.

This combined mechanism provides enhanced thermal regulation, improved temperature distribution, and increased system reliability for the battery module in NEVs. Shen et al. [26] proposed a hybrid method combining PCM with a liquid BTMS. Under high C-rate conditions, the findings indicate that integrating PCM with the liquid-based system reduced temperature non-uniformity by 41.67 % compared to a standalone liquid cooling BTMS. Similarly, Tan et al. [27] explored the effects of incorporating a PCM-liquid hybrid approach and found that the combined strategy, together with the optimized cooling structure, demonstrated strong potential for TMP. In further confirmation of the combined strategy's effects on thermal regulation for LIBs in NEVs, An et al. [28] investigated a hybrid system incorporating PCM-LCP with spatial channels. They maintained the battery temperature below 43.83 °C under 3 C-rate conditions, highlighting that the hybrid approach is a promising pathway to control the operating temperature of the battery in NEVs.

However, the practical application of conventional PCMs is limited by their inherently low thermal conductivity, which restricts effective HT and decreases overall system efficiency [29,30]. Furthermore, the use of PCM as a standalone cooling solution has an inherent drawback: once it has completely melted, its ability to absorb heat ceases, which can lead to a rise in battery temperature, especially in high ambient environments [31]. Consequently, PCM-based cooling systems typically need to be supplemented with an active cooling mechanism. Choi et al. [32] conducted comparative studies on thermal management approaches. They found that while PCM alone struggled with unacceptable temperature non-uniformity inside the battery, it could still maintain the maximum temperature within a safe range. In contrast, the fin-cooling approach even failed to keep the maximum temperature within the desired limits.

To overcome the aforementioned challenges, recent studies have focused on the development of composite phase change material (CPCM) with enhanced thermal properties. The coupling of high thermal conductivity materials, such as metal foams, metal-fins, nanofluids, graphene, and expandable graphite, has demonstrated a remarkable avenue in improving both HT capability and energy storage performance [33,34]. For example, Zhao et al. [35] proposed a hybrid-BTMS incorporated copper foam CPCM with liquid cooling, demonstrating significant improvement in controlling the operating temperature across the module. Moreover, Tong et al. [36] proposed a honeycomb LCP–PCM configuration with Al-fins to enhance heat transfer, which was able to limit

 doi:10.20944/preprints202605.1153.v1

the maximum temperature to 60 °C and maintain temperature non-uniformity within 5 °C under extremely unfavorable operating conditions. Likewise, Balasubramanian et al. [37] incorporated nanoparticles into paraffin to enhance its thermal conductivity and compared the thermal performance with that of a passive approach under a 3 C discharge rate. The study concluded that the hybrid strategy reduced the maximum temperature by 10.35 °C. Furthermore, Mane et al. [38] proposed a CPCM prepared by incorporating Fe_3O_4 nanoparticles into paraffin and found that the maximum temperature was reduced by 11.2 °C compared with a single-mode cooling technique.

In particular, metal foams, such as copper and aluminum foams, offer a porous structure that improves heat conduction and promotes even temperature distribution within the PCM matrix. Khaboshan et al. [4] examined the TMP of a hybrid BTMS configured with PCM, metal foam, and fins under a 3C-rate. They found that the hybrid system reduced the maximum temperature and temperature non-uniformity by 2 K and 66 %, respectively, under harsh circumstances, compared with PCM alone. This underscores that incorporating metal foam into PCM demonstrates strong potential for controlling battery temperature. The high conductivity of copper, coupled with PCM latent heat absorption, significantly enhances the HT performance of the system. Nevertheless, its weight and cost impose notable trade-offs and challenges. Wang et al. [39] examined the TMP of PCM–copper foam for 21700-type LIBs under 2 C discharge and found that the maximum temperature was controlled to marginally above 30 °C. Similarly, Yang et al. [40] studied the effects of incorporating PCM–Al foam into a liquid BTMS for prismatic LIBs under 2 C discharge, revealing that the proposed hybrid configuration reduced pumping power by 50 % compared to active liquid BTMS, while achieving the same TMP.

Apart from recent advancements, there remains a relative scarcity of comprehensive studies that systematically integrate CPCM with liquid-based BTMS while thoroughly exploring their combined thermal effects. In this context, the design and optimization of advanced hybrid BTMS configurations are crucial to fully exploit the potential of combined cooling strategies. Thus, this study proposes a novel synergistic hybrid CPCM–liquid-based BTMS for a cylindrical battery module operating at a 5 C discharge rate. The system integrates composite PCM embedded with Al-foam with a liquid cooling system, thereby enhancing thermal conductivity and improving HT capability. Three different LCP configurations, including serpentine-shaped, straight, and leaf-shaped, are designed and systematically evaluated, and based on their temperature regulation, uniformity, and hydraulic performance, the best-performing configuration is selected for further FCT optimization to improve overall cooling efficiency. Additionally, the effects of CFS and ambient temperature are analyzed. Finally, the performance of the proposed hybrid CPCM-liquid system is further assessed against a single-mode configuration employing CPCM alone. Overall, the proposed hybrid BTMS aims to offer a promising pathway for addressing the thermal challenges associated with high-power LIB systems, thereby ensuring safety, reliability, and operational performance in NEVs.

2. Physical Model and Numerical Methodology

2.1. Physical Model of Hybrid CPCM-Liquid BTMS

To investigate the TMP of the BTMS under high-load operating conditions, an 18650-type LIB is selected for this study due to its widespread use in practical applications. **Figure 1** illustrates the schematic configuration of the 3D battery system developed using SolidWorks. The proposed 3D hybrid BTMS model consists of four primary components: 18650-type cylindrical cells, CPCM, LCPs, and coolant flow channels. The battery cells are embedded within a CPCM–Al foam matrix, which serves as a thermal buffer to regulate temperature fluctuations. The cells are arranged in a 3 × 5 configuration to form a single battery module, ensuring a compact and realistic structural layout. In this design, the CPCM layer is strategically positioned between the battery cells, and the LCPs are made from aluminum due to its low density, high conductivity, and fabrication simplicity. During battery operation, the heat generated by electrochemical reactions is initially absorbed by the CPCM due to its high latent heat capacity. This phase change process effectively limits the temperature rise

 doi:10.20944/preprints202605.1153.v1

and enhances thermal uniformity across the module. Subsequently, the absorbed heat is transferred to the LCPs, where it is removed by the circulating coolant. Water is selected as the coolant in this study. The coolant flows through the embedded channels within the LCPs, facilitating continuous heat removal from the system and thereby improving overall cooling efficiency. This hybrid approach combines the advantages of passive (PCM-based) and active (liquid cooling) thermal management strategies. The detailed geometric dimensions of the hybrid BTMS configuration are presented in **Figure 1,** while the thermo-physical properties of the battery, PCM, LCP, and water are summarized in **Table 1.**

To reduce computational cost while preserving solution accuracy, a symmetric computational domain is employed. Based on heat-transfer symmetry, only a representative module consisting of five cells in a 1P5S (one parallel, five series) configuration is considered. The corresponding computational domain is illustrated in **Figure 1b.** Furthermore, three LCP geometries, serpentine-shaped, straight, and leaf-shaped designs, are systematically evaluated to assess their TMP. The comparison is based on key performance metrics, including maximum cell temperature, temperature non-uniformity, PCM activation, and pressure drop across the cooling channels. These parameters are essential for ensuring effective thermal regulation and hydraulic efficiency. In addition, the FCT of the selected LCP configuration is further analyzed to optimize the heat transfer characteristics and overall cooling performance.

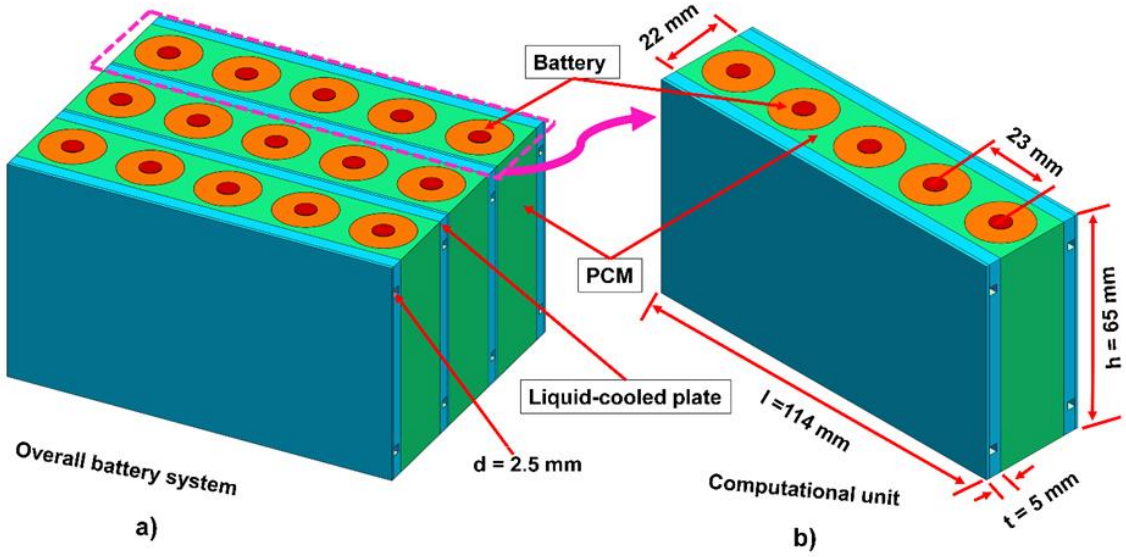

Figure 1. Schematic configuration of hybrid CPCM-liquid BTMS: **a)** Overall battery system, **b)** computational unit.

Table 1. Thermo-physical properties of the materials [24,35,40,41].

Materials Properties	RT35HC	Battery	water	LCP
Density solid (kg/m³)	880	2055		2719
Density liquid (kg/m³)	770		998.20	
Heat capacity (J/kg.K)	2000	1299	4182	871
Latent heat (kJ/kg）	247.60			
Thermal conductivity (W/m.K)	PCM= 0.20	λ_{radial} = 1.1	0.60	202.40
	CPCM = 5.62	λ_{axial} = 12.5		
Meshy zone (K)	304.15–310.15			
Solidus temperature T_s (K)	304.15			

 doi:10.20944/preprints202605.1153.v1

Liquidus temperature T_l (K)	310.15

2.2. Numerical Model and Governing Equations

2.2.1. Battery HG (Heat Generation) Model

The Parameters of the 3D LIB employed in this study are provided in **Table 2.** Owing to its multilayer wound construction, the battery possesses anisotropic thermal conductivity, which is specified in the axial, radial, and circumferential directions. A reference coordinate system is assigned to each battery within the computational domain to ensure accurate modeling. The material properties of the LIB components are presented in **Table 3.** Despite the inherent complexity of battery HG during charging/discharging, this study employs the simplified Bernardi model, widely used for battery thermal analysis, to determine the heat source. To establish a computationally efficient battery HG model, the heat generation is assumed to occur solely within the battery core, with any HG in other components neglected. The effect of thermal contact resistance between different components is also assumed to be negligible. Based on these assumptions, the battery's HG and thermal behavior are modeled through the energy equation [42]. The coupled electrochemical–thermal characteristics of the LIBs can be captured by this governing equation and can be estimated as:

$$\rho_b C_{P,b} \frac{\partial T_b}{\partial t} = \nabla.(\lambda_b \nabla T_b) + Q_{gen} \qquad (1)$$

where ϱ is the density (kg/m^3), C_P is the heat capacity (J/kg.K), λ is the thermal conductivity (W/(m.K), and T is the temperature (K). The subscript b is the battery material. Q_{gen} represents the heat generated in the battery (W/m^3).

The total heat (Q_{gen}) produced in a LIB is the sum of irreversible heat, reversible heat (entropic heat), and joule heating (ohmic heating) [43,44]. Irreversible heat (Q_{irr}) is produced by electrochemical reactions and ohmic losses during operations. Q_{irr} can be expressed as:

$$Q_{irr} = I(U_{ocv} - U) \qquad (2)$$

where I denote the discharge/charge current of the cell (A) and U represents the battery's voltage (V). The subscript ocv refers to the open circuit voltage.

Reversible heat is caused by the entropy change during charging and discharging. Q_{rev} can be calculated as:

$$Q_{rev} = -IT \frac{\partial U_{ocv}}{\partial T} \qquad (3)$$

Joule heating arises from the internal resistance of the battery and is proportional to the square of the current (I^2R), becoming particularly significant under high current operating conditions. Joule heating (Q_{joule}) can be expressed as:

$$Q_{joule} = -I^2 R \qquad (4)$$

where R is the battery internal resistance (Ω).

2.2.2. Heat Transfer (HT) Model

In the CPCM modeling, natural convection within the composite PCM–Al foam is neglected to simplify the analysis. This assumption is consistent with widely adopted approaches in the literature, where conduction-dominated HT is considered sufficient for metal-foam-enhanced PCM [40]. The unsteady phase change process of the CPCM is modeled using the enthalpy–porosity method. In this approach, the mushy zone is considered as a porous matrix, in which the liquid fraction represents the porosity of the material. The mushy zone constant was set to 10^5 in this study, as suitable values typically range from 10^3 to 10^8 depending on the PCM types and their boundary conditions, which is consistent with values reported in the literature [45]. As the phase transition progresses from solid to liquid, the porosity varies continuously from 0 (fully solid) to 1 (fully liquid). This formulation

 doi:10.20944/preprints202605.1153.v1

enables the incorporation of latent heat effects into the energy equation while implicitly capturing the phase interface evolution. Furthermore, the coolant is assumed to be an incompressible fluid. The maximum inlet velocity applied in this study is 0.10 m/s. At this velocity, the Reynolds number does not exceed 250 in any scenario, highlighting that the flow in the LCP channels is considered laminar (Re < 2300).

Under the above-mentioned assumptions, the HT within the LCP as well as the composite PCM–Al foam system is governed by the following set of equations [24]:

$$\rho_{cp} C_{P,cp} \frac{\partial T_{Cp}}{\partial t} = \nabla . \left(\lambda_{cp} \nabla T_{cp}\right) \quad (5)$$

$$\rho_{pcm} \frac{\partial H}{\partial t} = \nabla . \left(\lambda_{CPCM} \nabla T\right) \quad (6)$$

where ϱ is the density (kg/m³), C_p is the heat capacity, H is the enthalpy (J/kg), λ is the thermal conductivity (W/(m.K), and T is the temperature (K). The subscripts cp, PCM, and CPCM denote the cold plate, phase change material, and enhanced composite PCM-Al foam, respectively.

The enthalpy of composite PCM can be expressed as the sum of total enthalpy (H) and sensible enthalpy (h_s):

$$H = \Delta H + h_s \quad (7)$$

$$\Delta H = \beta L_h \quad (8)$$

$$h = h_r + \int_{T_o}^{T_{PCM}} C_{p,PCM} dT \quad (9)$$

where the terms ΔH represent PCM latent enthalpy change, h_s is sensible enthalpy, h_r is reference enthalpy, and Cp is the specific heat. T_o and T_{PCM} are the ambient temperature and the PCM temperature. Meanwhile, L_h and β denote the latent heat and liquid fraction, respectively.

The liquid fraction can be defined as [35]:

$$\beta = \begin{cases} 0, & T_{PCM} < T_s \\ \frac{T_{PCM} - T_s}{T_l - T_s}, & T_s < T_{PCM} < T_l, \\ 1, & T_{PCM} > T_l \end{cases} \quad (10)$$

Here, T_s and T_l correspond to the solidus temperature and liquidus temperature, respectively.

Enhanced thermal conductivity of the CPCM-Al foam can be expressed as follows [40,46]:

$$\lambda_{eff} = \frac{L_A + L_B + L_C + L_D}{R_A + R_B + R_C + R_D} \quad (11)$$

$$\begin{cases} R_A = \dfrac{4dL}{[2e^2 + \pi d(1-e)]\lambda_{Al} + \{4 - [2e^2 + \pi d(1-e)]\}\lambda_{PCM}} \\ R_B = \dfrac{(e-2d)L}{e^2\lambda_{Al} + (2-e^2)\lambda_{PCM}} \\ R_C = \dfrac{\left(\sqrt{2}-2e\right)L}{\pi d^2\lambda_{Al}\sqrt{2} + \left(2 - \pi d^2\sqrt{2}\right)\lambda_{PCM}} \\ R_D = \dfrac{2eL}{e^2\lambda_{Al} + (4-e^2)\lambda_{PCM}} \end{cases} \quad (12)$$

The porosity of the open-cell Al (metal) foam can be determined [47]:

$$\varepsilon = 1 - \frac{\sqrt{2}}{2}\left[\frac{3}{2}e^3 + \frac{3}{2}\pi d^2\left(1 - e\sqrt{2}\right) + 3(\pi - 2)d^3\right] \quad (13)$$

Here, R is a thermal resistance, L represents the node-to-node length, and ε represents the porosity of the open-cell Al foam, which is taken as 0.92 in this study. The subscripts A, B, C &D are different layers or (unit cell subsections). The parameters d and e represent the dimensionless foam ligament radius and cubic node edge length, respectively, where $e = f\,d$. Here, f is a dimensionless parameter

 doi:10.20944/preprints202605.1153.v1

determined as the ratio of node edge length to ligament radius ($f = r/a$), and d can be determined from Equation (13).

The coolant flow within the channel is resolved by solving the continuity equation (mass conservation), the Navier-Stokes equation (momentum conservation), and the energy conservation equation [48].

The continuity equation:

$$\frac{\partial \rho_c}{\partial t} + \nabla.(\rho_c \vec{v}) = 0 \qquad (14)$$

The momentum equation:

$$\frac{\partial}{\partial t}(\rho_c \vec{v}) + \nabla(\rho_c \vec{v}.\vec{v}) = \nabla.(\mu_c \nabla \vec{v}) - \nabla P + \rho_c \vec{g} \qquad (15)$$

Where μ is the dynamic viscosity (Pa.s), and P is the static pressure (Pa) of the coolant.

The energy equation:

$$\rho_c C_{P,c} \frac{\partial T_C}{\partial t} + \rho_c C_{P,c}(\vec{v}.\nabla T_c) = \nabla.(\lambda_c \nabla T_c) \qquad (16)$$

Where ϱ is the density, C_P is the heat capacity, λ is the thermal conductivity, T is the temperature, and $\vec{v}$, is the flow velocity (m/s). The subscript c denotes the coolant used in the BTMS.

The Reynolds number (Re) is determined as:

$$Re = \frac{\rho v_f . d_c}{\mu} \qquad (17)$$

Where v_f and d_c, are the flow velocity and the diameter of the channel.

Table 2. Thermo-physical parameters of 3D 18,650 type battery.

Parameters	Specifications	Unit
Dimension	Φ18 × 65	mm
Rated capacity	2.60	Ah
Nominal voltage	3.70	V
Minimum stop voltage	2.75	V
Maximum stop voltage	4.20	V
Weight	45	g
Cathode material	$LiNi_{0.8}Co_{0.15}Al_{0.05}O_2$	
Cathode material	Graphite	

Table 3. Material properties of 18,650 type battery [24,41].

Parameter	Thickness (μm)	ϱ (kg/m3)	Cp (J/kg.K)	λ(W/m.K)
Positive current collector	20	2770	875	170
Cathode	150	2328.50	1269.20	1.60
Separator	30	1009	1978.20	0.40
Negative current collector	14	8933	385	398
Anode	120	1347.33	1437.40	1.10

2.3. Simulation Method and Boundary Conditions

A transient model is developed in ANSYS Fluent to solve the governing equations for the hybrid PCM-BTMS. The coupled algorithm is employed for velocity–pressure coupling, offering a combination of numerical stability and high accuracy throughout the simulations. Spatial discretization is performed using a least-squares cell-based method for gradient reconstruction. The

 doi:10.20944/preprints202605.1153.v1

momentum, pressure, and energy equations are discretized using second-order upwind schemes. Convergence criteria are specified as 10^{-6} for the continuity equation, as well as for the momentum and energy equations. The under-relaxation factors are 0.70 for momentum and pressure, 0.90 for liquid fraction, and 1.0 for energy. The simulation is performed with a time-step size of 1 s, a maximum of 20 iterations per time step.

The following boundary conditions and simulation parameters were applied:

- The simulations were conducted over a range of inlet temperatures from 291.15 K to 309.15 K, in increments of 6 K, along with various CFS to enable a comprehensive parametric analysis.
- A uniform velocity inlet condition was applied at the channel inlet, while a pressure outlet boundary condition with a gauge pressure of 0 Pa was prescribed at the channel outlet.
- A no-slip condition was prescribed at the coolant–LCP interfaces.
- The battery cell–PCM interface was modeled as a thermally coupled wall, with thermal contact resistance neglected.
- The PCM-LCP as well as coolant interfaces were also treated as thermally coupled walls to account for conjugate heat transfer.
- All other walls of the LCPs and battery cells were assumed adiabatic.
- The external surfaces of the batteries were subjected to natural convection, with a convective heat transfer coefficient of 5 W/(m^2.K).

In this study, an RT35HC PCM (a paraffin wax) combined with Al-foam was employed. This material selection was motivated by its high latent heat, long-term stability, less degradation, and favorable mushy zone characteristics, making it particularly suitable for thermal management in LIBs to maintain optimal operating temperatures [24].

2.4. Grid Independence Verification

Systematic grid validation was performed to balance computational reliability and efficiency, as well as to confirm that additional mesh refinement had no significant influence on the simulation results. Five mesh sizes were examined, with grid counts of 276,304; 398,654; 1,584,577; 2,625,601; and 5,036,600 elements. **Figure 2a** depicts the final mesh model for the computational unit. The validation test was conducted under a 5 C discharge rate, using a serpentine LCP, at a CFS of 0.06 m/s and an inlet temperature of 298.15 K. As illustrated in **Figure 2b,** once the grid count exceeded 1,584,577 elements, the maximum temperature deviation was less than 0.002 K, confirming that further increases in mesh resolution had no significant impact on the simulation outcomes. Accordingly, the grid model with 1,584,577 elements was adopted for all subsequent simulations in this study.

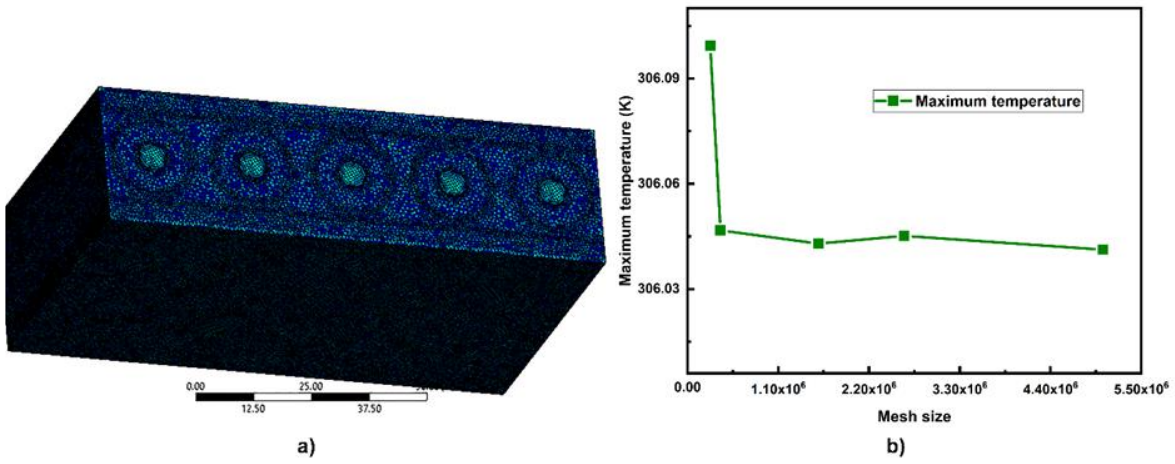

Figure 2. Scheme of: **a)** Mesh model, **b)** Maximum temperature with different grid sizes

 doi:10.20944/preprints202605.1153.v1

2.5. Model Validation

This section presents the battery heat generation rate and associated temperature rise, aiming to validate their reliability and accuracy by comparison with the experimental data from a previously published study by Chen et al. [24]. The validation is carried out under various discharge rate conditions, specifically 1 C, 2 C, and 3 C, all at an ambient temperature of 288.15 K and 308.15 K. The battery used in this validation matches the material properties, geometrical specifications, and operating conditions of the experimental reference; details of the specifications are summarized in **Tables 1, 2,** and **3.** A visual comparison and verification of the results are provided in **Figures 3a** and **b.** Therefore, as clearly illustrated in the graph, the battery temperature curves obtained from the numerical simulations are in strong agreement with those from the experimental measurements. Across all tested discharge scenarios, the maximum temperature difference between the experimental and numerical results is no more than 1.10 K. The deviation between numerical and experimental results arises primarily because the model assumes ideal thermal contact and neglects thermal resistance, leading to higher predicted temperatures. Whereas, natural convection and heat dissipation through cabling and connections reduce the temperature rise in the experimental setup, resulting in lower measured values. Overall, a close level of agreement confirms that the developed numerical model is sufficiently accurate and reliable, thereby rendering it well-suited for subsequent performance analyses of the battery system.

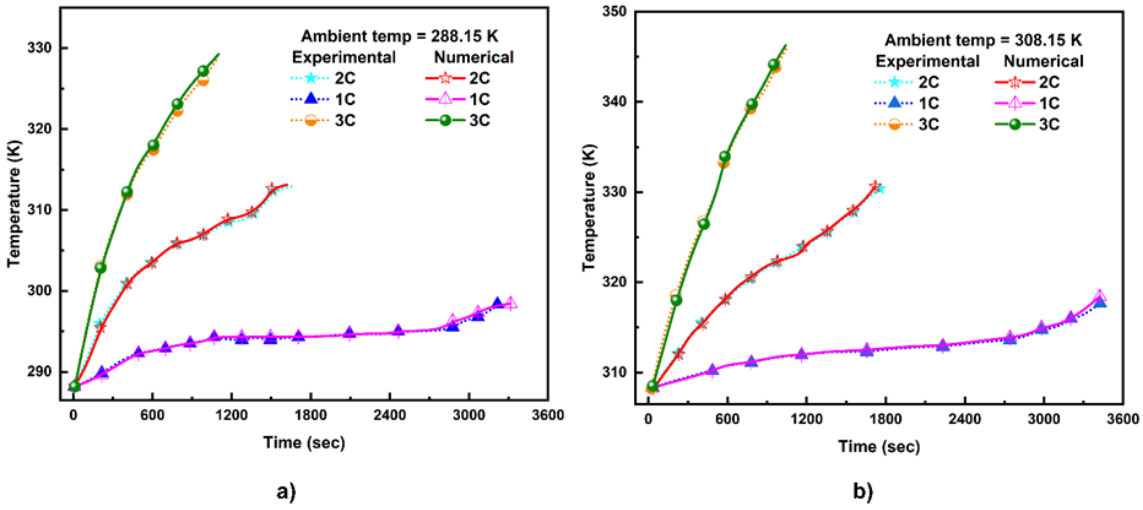

Figure 3. Comparison of numerical results with experimental results based on temperature rise under different working conditions.

3. Results and Discussions

This study presents a hybrid BTMS strategy that combines composite PCM with liquid cooling for cylindrical LIBs. The effectiveness of this approach in regulating module temperature is evaluated under diverse operating conditions, including extreme scenarios, to enhance TMP, safety, and service life through its thermal synergistic effect. In the subsequent sections, different LCP configurations are systematically assessed, and the most effective is selected to optimize FCT and enhance TMP. The effects of CFS and ambient temperature on maximum temperature, uniformity, and pressure drop are also analyzed at a 5 C discharge rate. Finally, the performance of the hybrid approach is evaluated and compared with that of the single-mode system utilizing CPCM alone.

3.1. Investigation of LCP Configurations

In this section, a comparative assessment is conducted under identical operating conditions to evaluate the effectiveness of LCP configurations integrated with a composite PCM–Al foam in a hybrid cooling system. Three LCP configurations, serpentine-shaped, straight, and leaf-shaped, are

 doi:10.20944/preprints202605.1153.v1

designed and analyzed in terms of key thermal performance indicators, including maximum temperature, temperature non-uniformity, liquid fraction, and pressure drop. As illustrated in **Figures 4a–c**, the nomenclature of each LCP configuration is derived from the geometry of its internal flow channels. The LCPs are symmetrically positioned on both sides of the CPCM layer, effectively sandwiching the CPCM and the battery. This arrangement facilitates efficient HT from the CPCM, which stores thermal energy, to the circulating coolant. Additionally, all LCP structures share the same overall dimensions, as detailed in **Figure 1b**, and their walls are in direct contact with the CPCM to enhance thermal conductivity. To ensure a fair comparison, all LCP schemes are designed with an identical channel diameter of 2.50 mm. The influence of LCP configuration on thermal regulation is investigated under consistent boundary conditions, including a CFS of 0.05 m/s, a coolant inlet temperature of 303.15 K, and a battery discharge rate of 5 C. These conditions enable a systematic comparison of the thermal and hydraulic performance of the proposed configurations.

Figure 5a compares the maximum battery module temperature under these three LCP configurations. The results demonstrate that all three configurations maintain the maximum temperature within a narrow range of 310.10 K to 310.49 K, indicating that each design provides adequate thermal regulation. Notably, the straight LCP achieves the lowest maximum temperature of 310.10 K, followed by the serpentine LCP at 310.29 K and the leaf-shaped LCP at 310.49 K. Compared to the leaf-shaped scheme, the straight LCP obtains a temperature reduction of 0.39 K, while the serpentine LCP achieves a reduction of 0.20 K. For further visualization, **Figure 6** presents the temperature contours of the battery module under the three LCP configurations, illustrating the temperature distribution across the module. Regarding temperature non-uniformity, **Figure 5a** also demonstrates that the temperature variation can be kept below 4.91 K, 4.92 K, and 5.27 K using the straight LCP, serpentine LCP, and leaf-shaped LCP, respectively. These results indicate that both the straight and serpentine LCPs achieve nearly identical temperature uniformity; however, the leaf-shaped LCP records a marginally higher temperature non-uniformity.

The overall efficiency of the BTMS depends not only on thermal regulation performance but also on energy utilization and pressure drop. As shown in **Figure 5b**, the serpentine LCP exhibits the highest pressure drop of 104.57 Pa, followed by the straight LCP at 26.35 Pa and the leaf-shaped LCP at 11.72 Pa. The longer coolant flow path in the serpentine design causes an increased pressure drop, which adversely affects its overall efficiency. Compared to the serpentine LCP, the leaf-shaped LCP reduces pressure drop by 88.79 %, while the straight LCP achieves a reduction of 74.80 %. These results indicate that the leaf-shaped LCP offers a distinct advantage by providing a balanced trade-off between thermal performance and hydraulic efficiency. Furthermore, the PCM melting and heat absorption capacity indicator, liquid fraction of the leaf-shaped LCP achieves the highest value of 29.30 %, compared to 12.40 % for the straight LCP and 16 % for the serpentine LCP **(Figure 5b).** Thus, due to its balanced benefits, including the lowest pressure drop and well control of OT under identical operating conditions, the leaf-shaped LCP is selected for further investigation in this study. However, it is noted that the temperature non-uniformity of the leaf-shaped design marginally exceeds the safe temperature non-uniformity threshold. To improve temperature uniformity and maintain temperature differences below safe limits, further investigations were performed by optimizing the FCT in the subsequent section.

 doi:10.20944/preprints202605.1153.v1

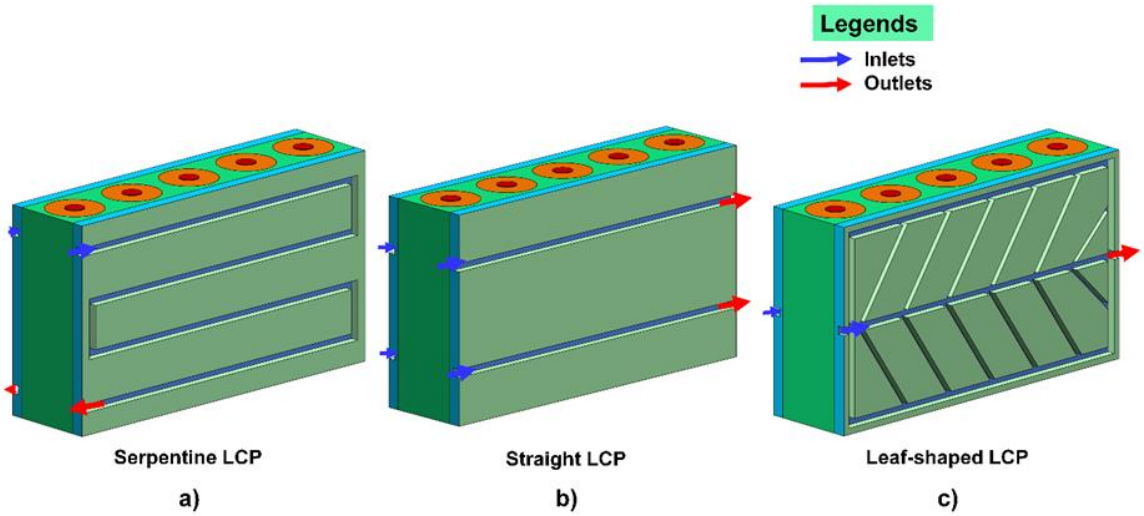

Figure 4. Different types of LCP schemes integrated with battery and PCM

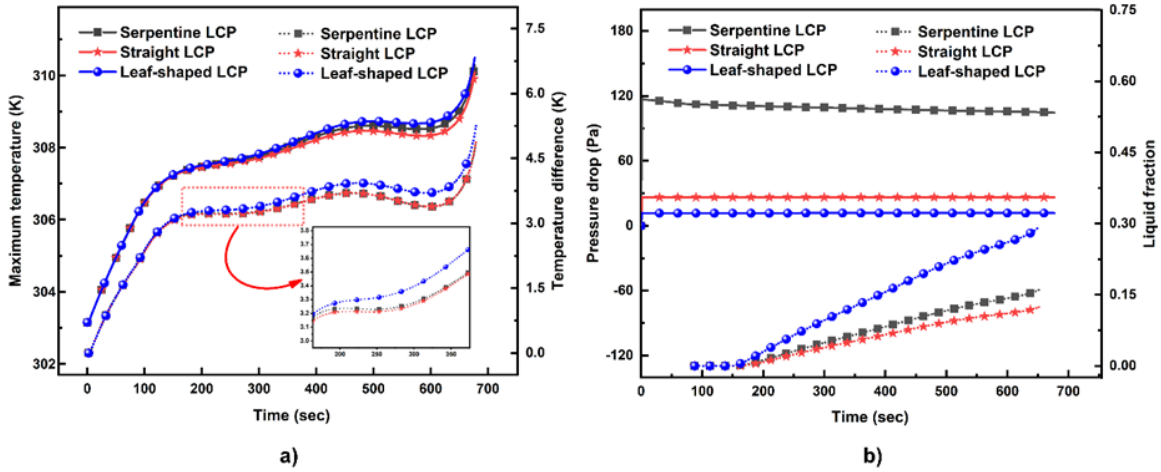

Figure 5. LCP configurations' performance effects on: **a)** Maximum temperature and temperature non-uniformity, **b)** Pressure drop and liquid fraction

 doi:10.20944/preprints202605.1153.v1

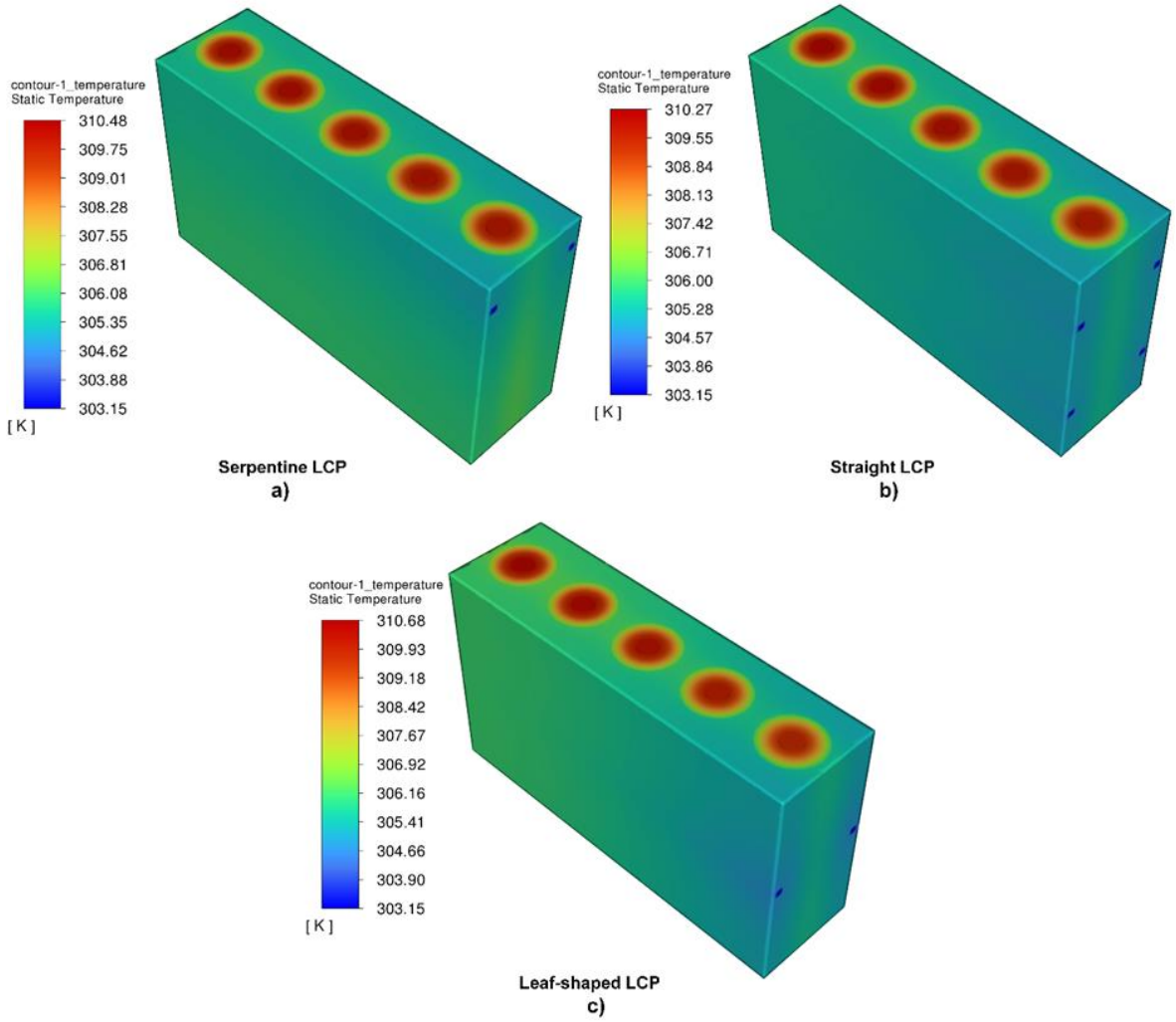

Figure 6. Battery temperature contours under the three LCP configurations.

3.2. Flow Channel Topology (FCT) Optimization

Based on the examination in the previous section, the leaf-shaped LCP is selected for further investigation and enhancement due to its balanced thermal management efficiency. Specifically, FCT optimization is pursued to improve thermal regulation capability and enable uniform, efficient HT. To achieve this, this section proposes and evaluates three different FCT schemes (FCT #1, FCT #2, and FCT #3), which vary in the position and number of flow channel inlets and outlets. Since two LCPs sandwich the battery and CPCM, each configuration is applied to both cold plates. As illustrated in **Figures 7a–c,** FCT #1 arranges one inlet and one outlet per side, totaling 2 inlets and 2 outlets across both LCPs. FCT #2 features two inlets and one outlet per side, also totaling 4 inlets and 2 outlets. FCT #3 features two inlets and two outlets per side, resulting in a total of 4 inlets and 4 outlets.

Figure 8a presents the maximum temperature of the battery module obtained under the three FCT schemes. The FCT #1(baseline scheme) records a maximum temperature of 310.49 K, while FCT #2 and FCT #3 achieve 309.98 K and 309.92 K, respectively. This corresponds to decreases of 0.51 K and 0.57 K, confirming that optimizing inlet/outlet topology enhances the TMP. More significantly, module temperature uniformity improved substantially, as shown in **Figure 8a.** FCT #2 achieves the lowest temperature variation of 4.87 K, representing a 7.60 % decrease compared to the baseline. Meanwhile, FCT #3 demonstrates a similar uniformity of 4.89 K (representing a 7.21 % reduction relative to the reference case). These marginal differences suggest that increasing inlet/outlet complexity beyond two inlets and one outlet per side offers diminishing returns for temperature distribution. For additional visual comparison, **Figure 9** presents the temperature contours, illustrating the temperature distribution inside the battery module under the three schemes.

 doi:10.20944/preprints202605.1153.v1

Regarding pressure drop, FCT #3 achieves the lowest value at 10.40 Pa, followed by FCT #1 at 11.72 Pa and FCT #2 at 21.33 Pa. A marked reduction in liquid fraction is observed, from 29.30 % (baseline) to 21.91 % when FCT #2 is employed and to 10.60 % when FCT #3 is applied. This behavior suggests that, while FCT #3 reduces flow resistance, it may also suppress PCM melting due to optimized flow distribution and more effective heat removal through active cooling. FCT #2, despite a slightly higher pressure drop, offers the best overall thermal uniformity and a reasonable peak temperature. In summary, the analysis identifies FCT #2 as achieving the most balanced trade-off in thermal regulation and overall performance. Consequently, the subsequent section further investigates the thermal behavior of FCT #2.

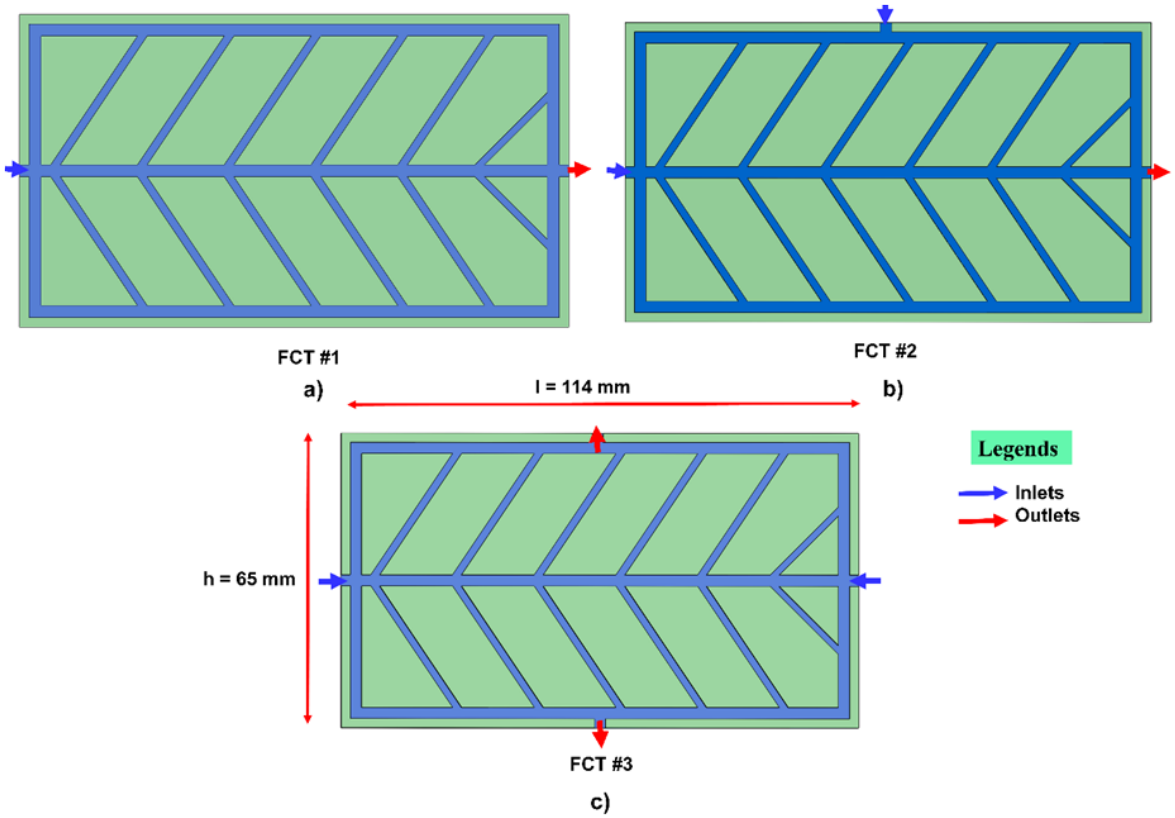

Figure 7. FCT optimization of leaf-shaped LCP: **a)** FCT #1, **b)** FCT #2, **c)** FCT #3

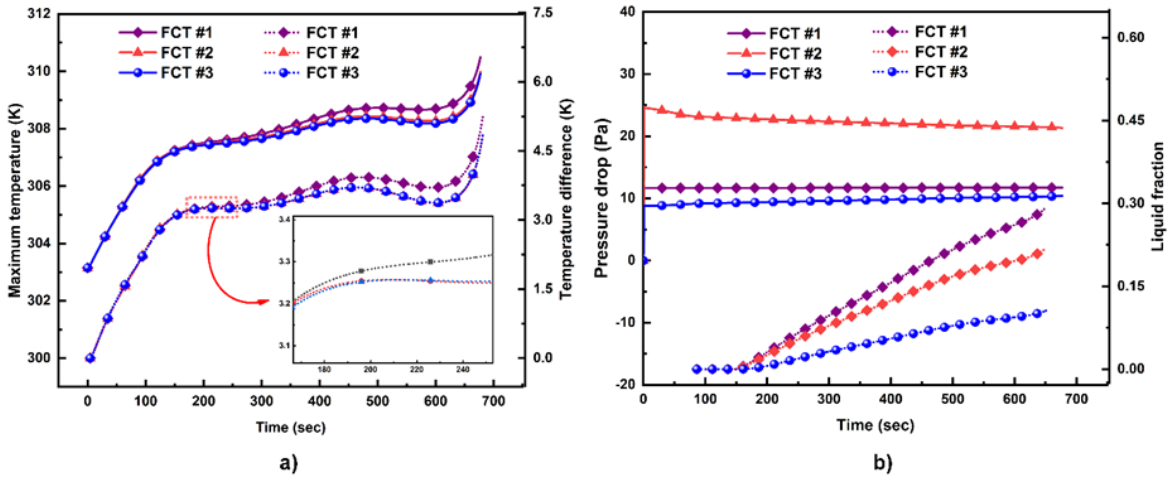

Figure 8. FCT optimization effects on: **a)** maximum temperature and temperature non-uniformity, **b)** pressure drop and sand liquid fraction

 doi:10.20944/preprints202605.1153.v1

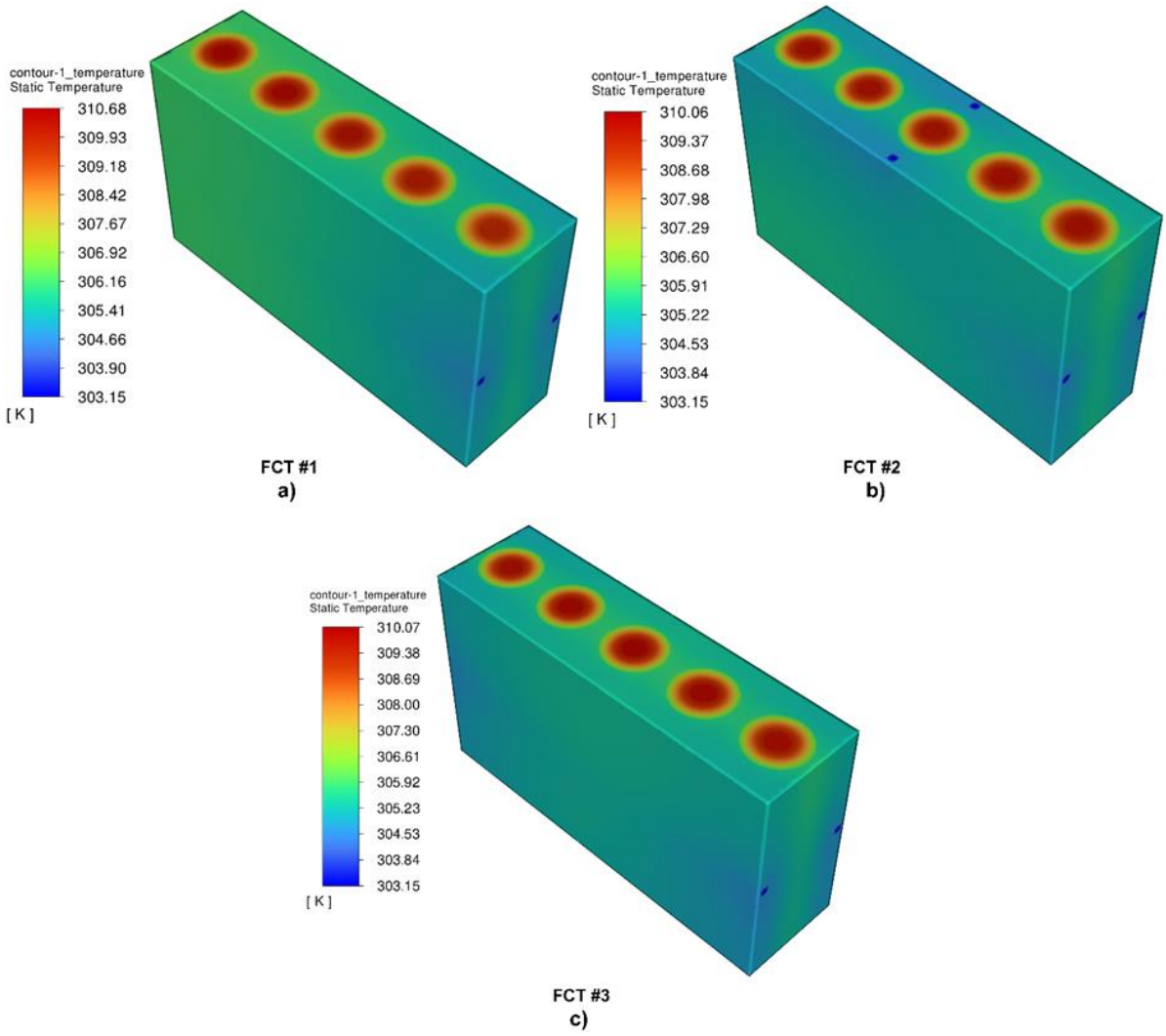

Figure 9. Battery temperature contours under the three FCT optimization.

3.3. Effects of the Coolant Flow Speed (CFS)

In this section, the effects of CFS on the BTMS are investigated. The results are illustrated in **Figures 10a** and **b**. It can be observed that the temperature of the battery module decreases from 310.32 K to 309.38 K as the CFS increases from 0.03 m/s to 0.10 m/s, corresponding to a reduction of 0.94 K in the maximum temperature. This indicates that higher CFS enhances heat dissipation. The battery module temperature distribution visualization is further illustrated via temperature contour (shown in **Figure 11**). The temperature non-uniformity initially exhibits a slight increase, rising from 4.80 K to 4.89 K as the CFS increases from 0.03 m/s, before decreasing to 4.79 K at 0.10 m/s. This trend is attributed to unevenly melting of PCM at moderate CFS, while at higher CFS, enhanced convection promotes more uniform heat dissipation. These findings are consistent with those reported by Zhao et al. [35]. Furthermore, the liquid fraction decreases with increasing CFS. Specifically, as the CFS increases from 0.03 m/s to 0.10 m/s, the liquid fraction is reduced from 28.65 % to 13.07 %, suggesting limited phase change activity due to improved convective HT and less heat load on PCM. This behavior is also similar to published results on PCM/forked LCP-based BTMs in reference [24]. Regarding the pressure drop, a linear increase is observed with increasing CFS, as shown in **Figure 10b.** When the CFS rises from 0.03 m/s to 0.10 m/s, the pressure drop significantly increases from 8.31 Pa to 66.88 Pa, indicating a higher pumping power requirement at elevated flow speeds.

 doi:10.20944/preprints202605.1153.v1

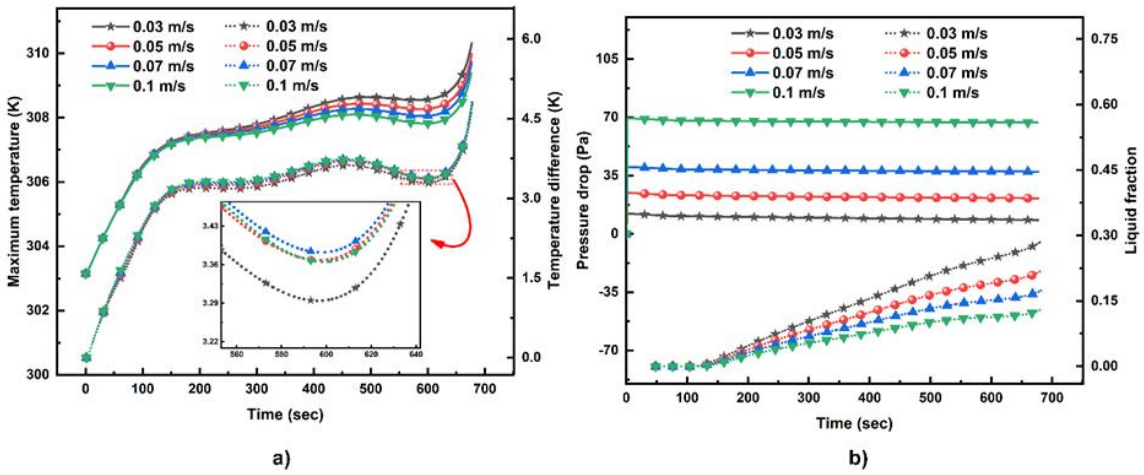

Figure 10. The effects of CFS on: **a)** Maximum temperature and temperature non-uniformity, **b)** Pressure drop and liquid fraction

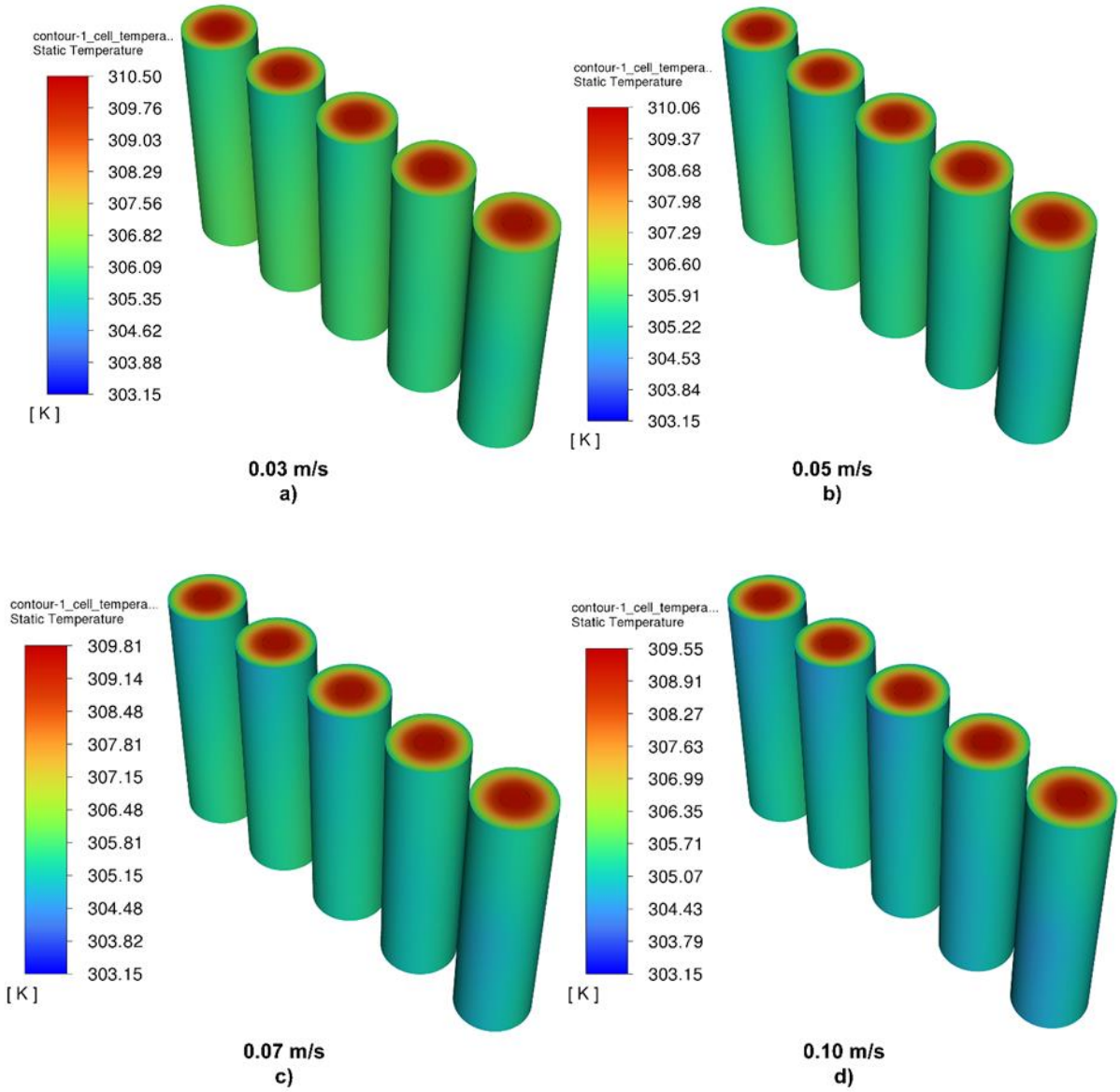

Figure 11. Temperature contour of the battery module under the effects of CFS.

 doi:10.20944/preprints202605.1153.v1

3.4. Investigation of Ambient Temperature Effects

To further evaluate the TMP of the proposed hybrid composite PCM-liquid BTMS, simulations were conducted under different ambient temperature conditions. The analysis was performed over a temperature range of 291.15 K to 309.15 K, with an incremental step of 6 K. The corresponding TMP results are presented in **Figure 12**. As the ambient temperature increases, both the maximum and minimum temperatures of the battery module rise accordingly. Specifically, the maximum temperature increases from 300.45 K to 315.77 K, while the minimum temperature increases from 295.03 K to 311.68 K, as the ambient temperature varies from 291.15 K to 309.15 K. This trend is expected due to the decreased temperature gradient between the cell and its surroundings at elevated ambient temperatures. In contrast, temperature non-uniformity decreases with increasing ambient temperature. The non-uniformity reduces from 5.61 K at 291.15 K to 4.27 K at 309.15 K, corresponding to a 23.89 % reduction. This improvement can be attributed to the enhanced utilization of PCM latent heat at elevated temperatures, where more homogeneous melting occurs throughout the module. These findings are also supported by the study reported [24]. The synergistic interaction between the CPCM and liquid cooling promotes more homogeneous heat absorption and distribution, even under high-temperature discharge conditions. For further insight, **Figure 13** illustrates the temperature contours of the battery module under different ambient conditions. The results show a more uniform temperature field at higher ambient temperatures, supporting the observed reduction in thermal gradients.

The pressure drop exhibits a decreasing trend with increasing ambient temperature, declining from 29.04 Pa to 14.93 Pa (a reduction of 48.59 %) as the temperature increases from 291.15 K to 309.15 K. This behavior is due to the temperature-dependent reduction in coolant viscosity, which lowers flow resistance and consequently reduces frictional losses and pumping power requirements within the cooling channels. Regarding the PCM melting behavior, the liquid fraction increases significantly with ambient temperature, rising from nearly 0 % (solid) at 291.15 K to approximately 100 % (liquid) at 309.15 K. The liquid fraction distributions shown in **Figure 14** further confirm that higher ambient temperatures increase extensive PCM melting. This indicates that the hybrid CPCM-liquid BTMS remains effective in utilizing latent heat storage even under elevated environmental conditions.

Besides, the maximum temperature distribution among individual cells within the module was analyzed to assess spatial variations. The cells are numbered sequentially from 1 to 5 along the flow direction, as illustrated in **Figure 12d.** It is observed that the highest temperatures consistently occur at the outlet side (Cell 5), while the lowest temperatures are recorded at the inlet side (Cell 1). For Cell 5, the maximum temperatures are 300.45 K, 305.65 K, 309.98 K, and 315.77 K at ambient temperatures of 291.15 K, 297.15 K, 303.15 K, and 309.15 K, respectively. In contrast, Cell 1 records lower temperatures of 299.94 K, 305.19 K, 309.66 K, and 315.44 K under the same conditions. Nevertheless, the temperature variation among individual cells remains minimal and well-controlled, as obviously shown in **Figure 12d.** The maximum temperature differences between the hottest and coolest cells are 0.51 K, 0.46 K, 0.32 K, and 0.33 K at ambient temperatures of 291.15 K, 297.15 K, 303.15 K, and 309.15 K, respectively. These values are significantly lower than the recommended limits for temperature variation within battery modules, indicating excellent thermal uniformity. This demonstrates that the proposed hybrid CPCM-liquid BTMS effectively regulates the operating temperature across the module, even under harsh ambient conditions. Therefore, the system presents a promising solution for maintaining safe and uniform thermal conditions in LIBs, particularly in NEVs.

 doi:10.20944/preprints202605.1153.v1

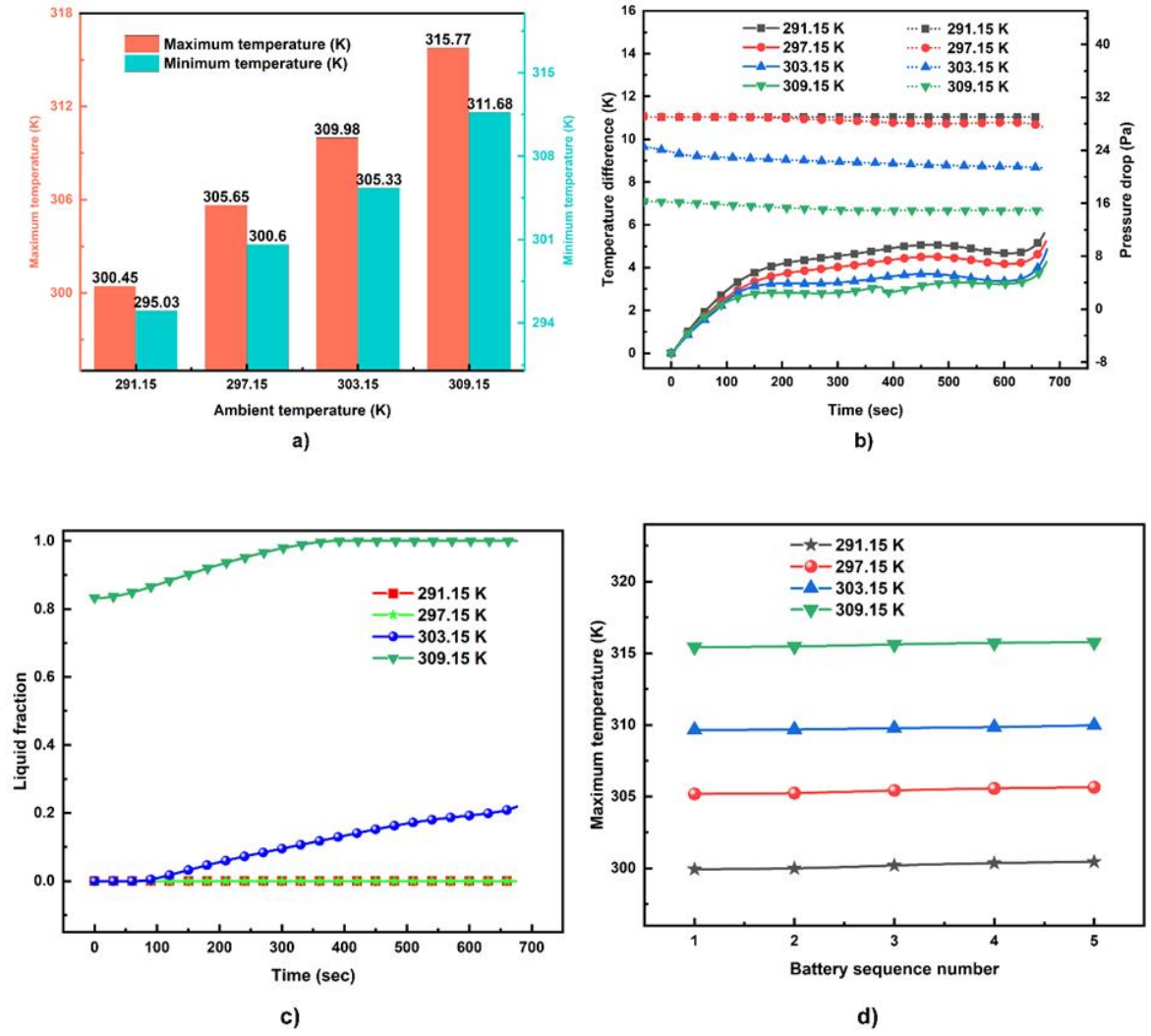

Figure 12. The effects of ambient temperature on: **a)** Maximum and minimum battery temperature, **b)** Temperature non-uniformity and pressure drop

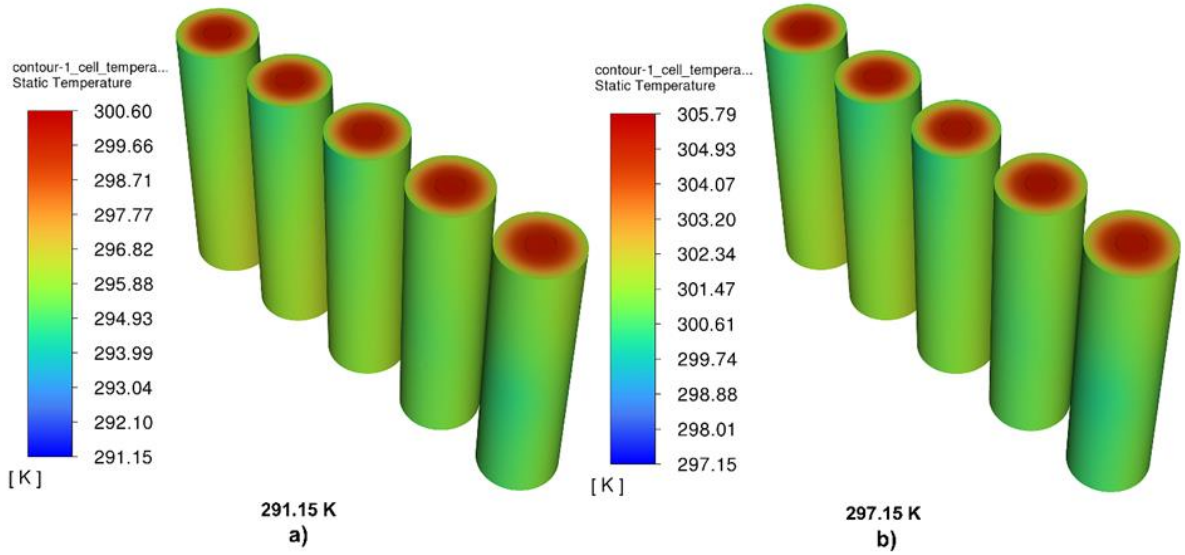

 doi:10.20944/preprints202605.1153.v1

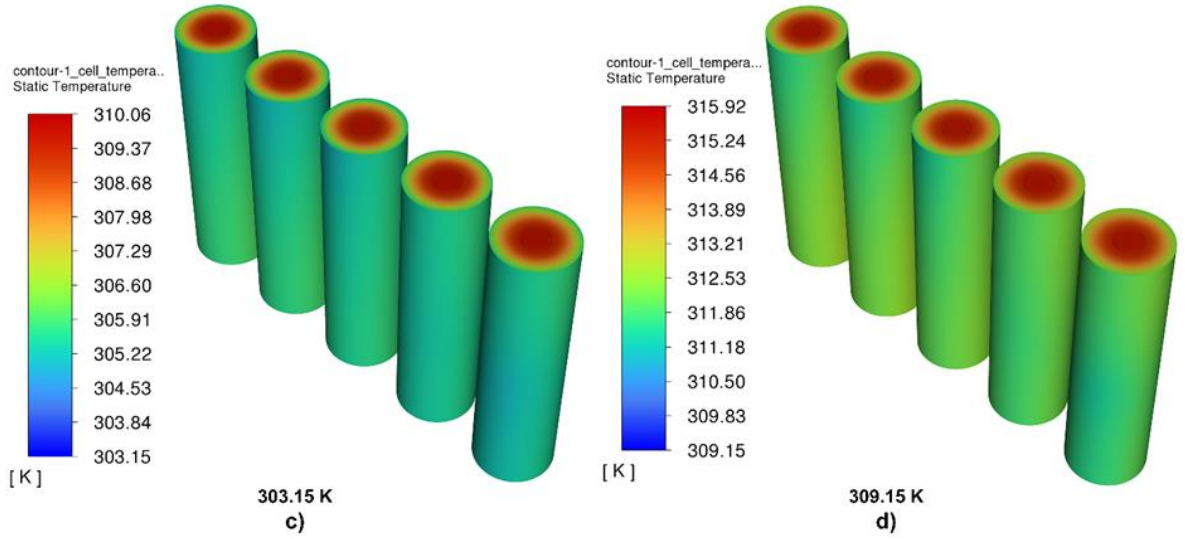

Figure 13. Temperature contour of the battery module under various ambient temperatures

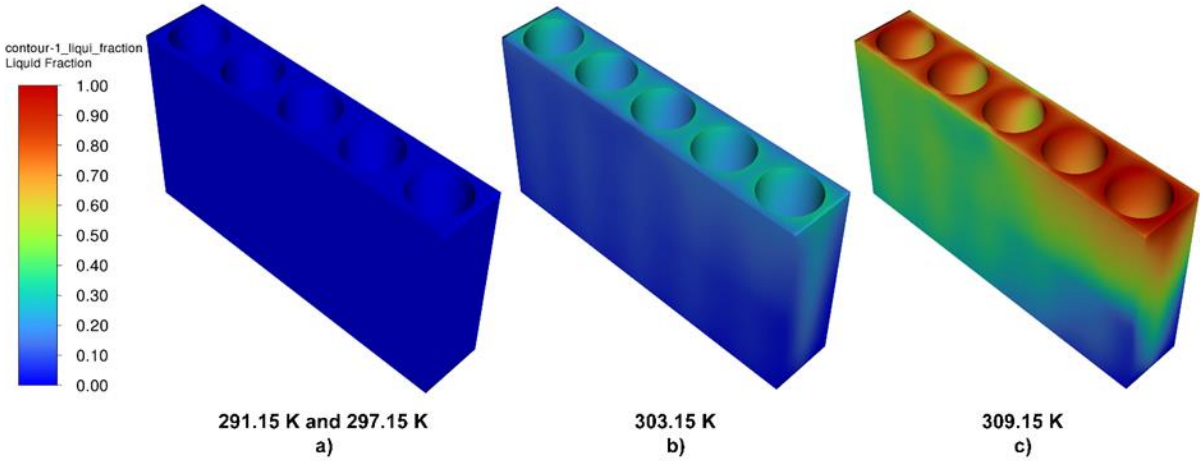

Figure 14. Liquid fraction contour of PCM melting distribution under various ambient temperatures

3.5. Performance Evaluation of CPCM-Only and Hybrid CPCM-Liquid BTMS Configurations

This section presents a comparative performance analysis of the hybrid CPCM–liquid approach and the CPCM-only approach. The analysis was conducted at ambient temperatures of 303.15 K and 309.15 K for both systems, and the corresponding simulation results are illustrated in **Figure 15.** At an ambient temperature of 303.15 K, the maximum module temperature is limited to 309.98 K and 311.42 K for the hybrid configuration and CPCM-only system, respectively. When the ambient temperature increases to 309.15 K, the maximum temperature rises to 315.77 K for the hybrid system and 324.58 K for the CPCM-only system. At 303.15 K, the liquid fraction in the CPCM-liquid BTMS decreases from 50.40 % to 21.91 % relative to the CPCM-only scenario, indicating that the incorporation of active (liquid) cooling notably dissipates heat and lowers the PCM melting rate. Overall, the proposed hybrid CPCM-liquid BTMS demonstrates superior thermal performance, maintaining lower temperatures level under both ambient conditions and reducing the maximum temperature by 8.81 K at 309.15 K compared to the CPCM-only configuration, thereby mitigating potential safety concerns. The enhanced performance of the hybrid system can be attributed to the combined effect of CPCM and liquid cooling, which promotes improved HT and offers efficient thermal uniformity under elevated thermal conditions.

In addition, the synergistic thermal performance of the hybrid CPCM–liquid BTMS is comparatively evaluated and validated against established thermal management approaches. The

 doi:10.20944/preprints202605.1153.v1

comparison is carried out in terms of maximum temperature and temperature variation under different discharge rates and ambient temperatures. The selected studies used for comparison are summarized in **Table 4**. As clearly indicated in **Table 4**, the present study demonstrates superior performance in regulating the OT, achieving a more even temperature distribution across the battery module compared to the referenced works. However, in certain cases, particularly under low discharge rates (e.g., 3 C), the current study exhibits slightly lower performance in controlling temperature difference. For instance, the results reported by Tan et al. [27] indicate a 1.30 K higher reduction in temperature variation compared to the present study. Nevertheless, the present study achieves a greater reduction in maximum temperature, with an improvement of 9.78 K relative to that work. A detailed comparison with each selected study is presented in **Table 4.** Overall, the comparison and validation results confirm the reliability and accuracy of the proposed numerical approach in predicting the thermal behavior of the battery module. Furthermore, the proposed hybrid CPCM–liquid BTMS exhibits enhanced TMP, including improved temperature regulation and uniformity, compared with previously reported configurations. These improvements indicate the strong potential of the proposed system to enhance battery thermal safety and prolong battery cycle life under high discharge operating conditions.

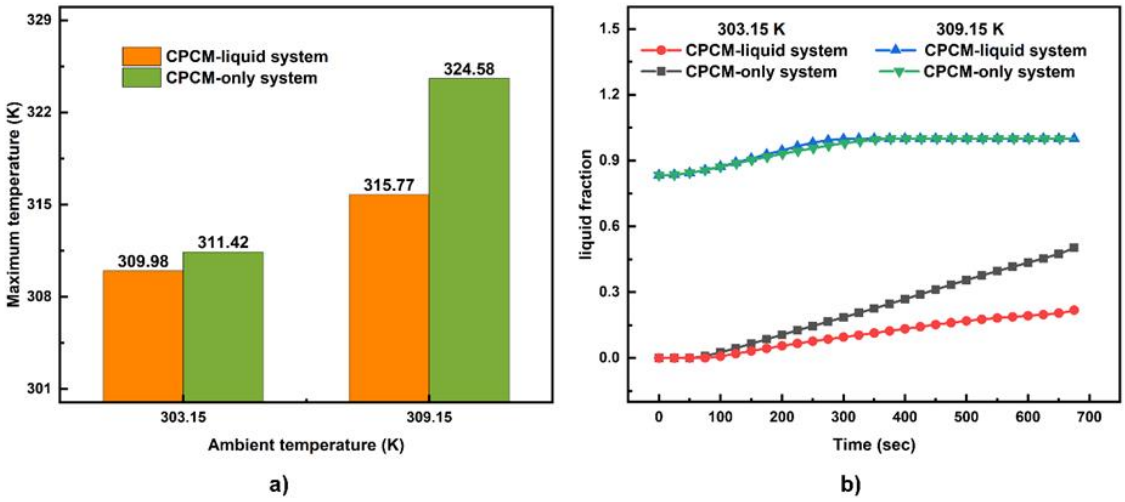

Figure 15. Evaluate Performance between the hybrid and CPCM-only system on: **a)** maximum temperature of the module, **b)** liquid fraction

Table 4. Validation and comparison of the TMP of the current studies with previously reported results.

Studies	BTMS strategies	Operating condition		Performance	
		C-rate	Tamb (K)	Tmax (K)	ΔT
Sun et al. [49]	CPCM + liquid	5	310	319.3	4.5
Tan et al. [27]	PCM + liquid	3	303.15	319.76	3.57
Luo et al. [50]	PCM + HP + TEC	5	303.15	316.78	4.09
Dhinesh et al. [37]	PCM + 10 % Al2O3 + liquid	3	301.15	313.96	-
Current study	CPCM + liquid	5	303.15	309.98	4.87
//	//	//	309.15	315.77	4.27

PCM = Phase change material, CPCM = Composite PCM, Tamb = Ambient temperature
TEC = Thermoelectric cooler, HP = heat pipe

4. Conclusions

This study proposes a hybrid BTMS that integrates composite PCM–Al foam with liquid cooling for cylindrical LIBs. To address the limitations of standalone cooling techniques in dissipating battery

 doi:10.20944/preprints202605.1153.v1

heat during operation, the present work comprehensively investigates the synergistic thermal performance of a hybrid CPCM-liquid BTMS. TMP is evaluated across a wide range of working environments, including extreme conditions. Various LCP configurations are assessed, with the optimal design selected and its FCT further optimized to improve overall performance. The effects of CFS and ambient temperature on OT, PCM melting, and pressure drop are also examined at a 5 C discharge rate.

The main findings are summarized as follows:

1. All three LCP configurations maintain maximum temperature and temperature uniformity within safe operating limits at a CFS of 0.05 m/s. The straight LCP achieves the lowest maximum temperature (310.10 K), followed by the serpentine (310.29 K) and leaf-shaped design (310.49 K). Temperature uniformity is similar for the straight and serpentine configurations (4.92 K and 4.91 K), while the leaf-shaped LCP slightly exceeds the recommended threshold (5.27 K). Despite this marginal deviation, the leaf-shaped LCP exhibits a substantially lower pressure drop (by 88.79 % compared to the serpentine). Thus, the leaf-shaped LCP offers the most favorable overall trade-off between TMP, hydraulic efficiency, and system effectiveness for the intended application.
2. The optimization of FCT is performed, and the FCT #2 configuration (featuring two inlets and one outlet per side) demonstrated the most balanced overall performance, achieving the lowest temperature variation (4.87 K) and a reduction in maximum temperature of 0.51 K compared to the baseline configuration (FCT #1). While FCT #3 exhibited the lowest pressure drop and a notable decrease in PCM liquid fraction, it is accompanied by a complex structural design. Overall, FCT #2 is identified as the optimal configuration, offering a superior balance between thermal regulation, energy efficiency, and system reliability.
3. Increasing the CFS from 0.03 m/s to 0.10 m/s reduces the maximum battery temperature from 310.32 K to 309.38 K (below 0.94 K reduction) and decreases the PCM liquid fraction from 28.65 % to 13.07 %, while temperature non-uniformity shows a slight variation (rises from 4.80 K to 4.89 K before reducing to 4.79 K); however, this enhancement is accompanied by a notable rise in pressure drop, indicating that an optimal CFS is necessary to balance thermal performance and pumping power in the hybrid CPCM–liquid BTMS.
4. Increasing the ambient temperature (291.15–309.15 K) results in a proportional rise in both the maximum and minimum battery module temperatures due to increased heat generation. In contrast, temperature non-uniformity decreases significantly (by 23.89 %), indicating improved thermal uniformity. Additionally, the pressure drop decreases markedly (by 48.59 %), while the PCM liquid fraction increases from nearly 0 % to 100 %, confirming the full activation of latent heat storage. The hybrid CPCM–liquid BTMS maintains effective thermal regulation even under harsh ambient conditions, highlighting its robustness and reliability.
5. The maximum temperature distribution among individual cells is also evaluated under varying ambient temperatures. The results show that the maximum cell-to-cell temperature difference remains very low (below 0.51 K), which is well within recommended limits, thereby demonstrating excellent thermal uniformity. However, a consistent temperature gradient is observed along the flow direction, with higher temperatures at the outlet side due to cumulative heat absorption by the coolant.
6. Under an ambient temperature of 309.15 K, the hybrid CPCM-liquid BTMS maintained the maximum temperature to 315.77 K, outperforming the CPCM-only configuration, which reached 324.58 K, indicating an 8.81 K increase that may raise safety concerns.

Overall, the proposed hybrid CPCM–liquid BTMS exhibits strong potential for advanced thermal management of LIBs in NEVs, particularly under high-temperature operating conditions, and provides valuable design insights for developing efficient and reliable BTMS for high-performance applications. Future work should focus on enhancing and optimizing the BTMS at the large-pack/system level, incorporating real-world operating conditions and leveraging intelligent

 doi:10.20944/preprints202605.1153.v1

control approaches to further improve TMP, safety, efficiency, and practical applicability in electric vehicle systems.

Funding: This study was funded by the Technology Research Project of Hunan Province of China (Grant No. 2023ZJ1050).

Data Availability Statement: The original contributions presented in this study are included in the article. Further inquiries can be directed to the corresponding author.

Conflicts of Interest: The authors declare no conflict of interest.

Abbreviations

The following abbreviations are used in this manuscript:

LIB	Lithium-ion battery
BTMS	Battery thermal management system
NEVs	New energy vehicles
LCP	Liquid-cooled plate
TMP	Thermal management performance
OT	Operating temperature
HT	Heat transfer
HG	Heat generation
TR	Thermal runaway
PCM	Phase change material
CPCM	Composite phase change material
CFS	Coolant flow speed
FCT	Flow channel topology
RT35HC	Rubitherm 35 high capacity

References

1. Wang, X., X. Dong, Z. Zhang, and Y. Wang, Transportation carbon reduction technologies: A review of fundamentals, application, and performance. Journal of Traffic and Transportation Engineering (English Edition) 2024, 11, 1340-77.https://doi.org/10.1016/j.jtte.2024.11.001.
2. Hasan, M.M., R. Haque, M.I. Jahirul, M.G. Rasul, I.M.R. Fattah, N.M.S. Hassan, et al., Advancing energy storage: The future trajectory of lithium-ion battery technologies. Journal of Energy Storage 2025, 120, 116511.https://doi.org/10.1016/j.est.2025.116511.
3. Njema, G.G., R.B.O. Ouma, and J.K. Kibet, A Review on the Recent Advances in Battery Development and Energy Storage Technologies. Journal of Renewable Energy 2024, 2024, 2329261.https://doi.org/10.1155/2024/2329261.
4. Najafi Khaboshan, H., F. Jaliliantabar, A.A. Abdullah, S. Panchal, and A. Azarinia, Parametric investigation of battery thermal management system with phase change material, metal foam, and fins; utilizing CFD and ANN models. Applied Thermal Engineering 2024, 247, 123080.https://doi.org/10.1016/j.applthermaleng.2024.123080.
5. Takiso, T.A. and J. Yu, Research progress on the optimization of thermal management systems for lithium-ion batteries in new energy vehicles. Journal of Energy Storage 2025, 134, 118144.https://doi.org/10.1016/j.est.2025.118144.
6. Oyewola, O.M., A.A. Awonusi, and O.S. Ismail, Design optimization of Air-Cooled Li-ion battery thermal management system with Step-like divergence plenum for electric vehicles. Alexandria Engineering Journal 2023, 71, 631-44.https://doi.org/10.1016/j.aej.2023.03.089.
7. Zhang, F., L. Zhang, A. Lin, P. Wang, and P. Liu, Multi-method collaborative optimization for parallel air cooling lithium-ion battery pack. International Journal of Energy Research 2022, 46, 14318-33.https://doi.org/10.1002/er.8145.

 doi:10.20944/preprints202605.1153.v1

8. Xiaoming, X., T. Wei, F.E.I. Jiaqi, H. Donghai, and S. Xudong, The forced air cooling heat dissipation performance of different battery pack bottom duct. International Journal of Energy Research 2018, 42, 3823 - 36. https://doi.org/10.1002/er.4114.
9. Chen, K., W. Wu, F. Yuan, L. Chen, and S. Wang, Cooling efficiency improvement of air-cooled battery thermal management system through designing the flow pattern. Energy 2019, 167, 781-90.https://doi.org/10.1016/j.energy.2018.11.011.
10. Singh, L.K., R. Kumar, and A.K. Gupta, A novel strategy of enhanced thermal performance in air cooled lithium-ion battery by wavy walls. Thermal Science and Engineering Progress 2023, 43, 101964.https://doi.org/10.1016/j.tsep.2023.101964.
11. Guo, Z., Y. Wang, S. Zhao, T. Zhao, and M. Ni, Investigation of battery thermal management system with considering effect of battery aging and nanofluids. International Journal of Heat and Mass Transfer 2023, 202, 123685.https://doi.org/10.1016/j.ijheatmasstransfer.2022.123685.
12. Mitra, A., R. Kumar, and D.K. Singh, Thermal management of lithium-ion batteries using carbon-based nanofluid flowing through different flow channel configurations. Journal of Power Sources 2023, 555, 232351.https://doi.org/10.1016/j.jpowsour.2022.232351.
13. Lai, Y., W. Wu, K. Chen, S. Wang, and C. Xin, A compact and lightweight liquid-cooled thermal management solution for cylindrical lithium-ion power battery pack. International Journal of Heat and Mass Transfer 2019, 144, 118581.https://doi.org/10.1016/j.ijheatmasstransfer.2019.118581.
14. Guo, Z., Q. Xu, S. Zhao, S. Zhai, T. Zhao, and M. Ni, A new battery thermal management system employing the mini-channel cold plate with pin fins. Sustainable Energy Technologies and Assessments 2022, 51, 101993.https://doi.org/10.1016/j.seta.2022.101993.
15. Buonomo, B., D. Ercole, O. Manca, and F. Menale, Thermal cooling behaviors of lithium-ion batteries by metal foam with phase change materials. Energy Procedia 2018, 148, 1175-82.https://doi.org/10.1016/j.egypro.2018.08.024.
16. Kumar, A., J.R. Senapati, and S. Acharya, Passive cooling of a lithium-ion battery pack using PCM and longitudinal/circular fins: A numerical study with experimental validation. Journal of Energy Storage 2025, 111, 115464.https://doi.org/10.1016/j.est.2025.115464.
17. Pal, R.K., J.K.S. Paw, P. Ganesan, and C.W. Tong, Modeling and simulation of phase change material-based passive and hybrid thermal management systems for lithium-ion batteries: A comprehensive review. Journal of Energy Storage 2025, 116, 116011.https://doi.org/10.1016/j.est.2025.116011.
18. Rahmani, A., M. Dibaj, and M. Akrami, Recent Advancements in Battery Thermal Management Systems for Enhanced Performance of Li-Ion Batteries: A Comprehensive Review. Batteries, Journal, 10(8)(2024) 265.10.3390/batteries10080265.
19. Lee, Y.-J., T.-G. Park, C.-H. Park, S.-J. Kim, J.-S. Lee, and S.-H. Rhi, Heat Pipe Integrated Cooling System of 4680 Lithium–Ion Battery for Electric Vehicles. Energies, Journal, 18(15)(2025) 4132.10.3390/en18154132.
20. Ammar, H., M. Delbani, F. Fardoun, B.E. Zoghbi, H. Mouzanar, J. Faraj, et al., Hybrid liquid–PCM thermal management for high–capacity lithium–ion batteries under fast charging: A parametric comparative study. Results in Engineering 2025, 27, 106674.https://doi.org/10.1016/j.rineng.2025.106674.
21. Wu, Z., H. Chen, L. Jiang, P. Zhang, Z. Ji, and D. Luo, Thermal management of lithium-ion batteries using a PCM-HP-TEC hybrid BTMS: A numerical study. International Communications in Heat and Mass Transfer 2025, 169, 109702.https://doi.org/10.1016/j.icheatmasstransfer.2025.109702.
22. Rahmani, A., M. Dibaj, and M. Akrami, Enhancing Battery Pack Cooling Efficiency Through Graphite-Integrated Hybrid-Battery Thermal Management Systems. Batteries, Journal, 11(3)(2025) 113.10.3390/batteries11030113.
23. Rabiei, M., A. Gharehghani, S. Saeedipour, A.M. Andwari, and J. Könnö, Proposing a Hybrid BTMS Using a Novel Structure of a Microchannel Cold Plate and PCM. Energies, Journal, 16(17)(2023) 6238.10.3390/en16176238.
24. Chen, X., Y. Su, Y. Zhang, J. Shen, X. Xu, X. Wang, et al., Performance of thermal management system based on PCM/forked liquid-cold plate for 18650 cylindrical battery. Journal of Energy Storage 2024, 91, 112071.https://doi.org/10.1016/j.est.2024.112071.

 doi:10.20944/preprints202605.1153.v1

25. Hyun, S.W., J.H. Kim, and D.H. Shin, Hybrid PCM–Liquid Cooling System with Optimized Channel Design for Enhanced Thermal Management of Lithium–Ion Batteries. Energies, Journal, 18(18)(2025) 4996.10.3390/en18184996.
26. Shen, C., C. Su, Z. Zhang, F. Wang, Z. Wang, and S. Wang, Synergistic PCM–Liquid Thermal Management for Large-Format Cylindrical Batteries Under High-Rate Discharge. Applied Sciences, Journal, 16(7)(2026) 3200.10.3390/app16073200.
27. Tan, Z., X. Wu, Z. Chen, J. Xiao, and S. Yang, Heat Dissipation and Structural Optimization of Cylindrical Lithium-Ion Batteries with Phase Change Material–Liquid Hybrid Cooling: A Numerical Study. Energies, Journal, 18(23)(2025) 6108.10.3390/en18236108.
28. An, Z., H. Zhong, H. Liu, and Z. Gao, Performance evaluation on liquid-PCM hybrid battery thermal management with spatial network flow channels. Journal of Energy Storage 2025, 118, 116251.https://doi.org/10.1016/j.est.2025.116251.
29. Tan, S., Y. Huang, F. Zhang, J. E, and X. Song, Effect of variable cross-section liquid cooling pipes on thermal management performance enhancement of lithium-ion batteries. Energy 2025, 334, 137649.https://doi.org/10.1016/j.energy.2025.137649.
30. Hussien, S.A., A.B.M. Ali, O.J. Alkhatib, and I. Mahariq, Enhanced passive thermal management of lithium-ion batteries with conical cylindrical chamber incorporating various phase change materials. Scientific Reports 2025, 15, 35675.10.1038/s41598-025-19597-0.
31. Calborean, A., L. Máthé, and O. Bruj, Phase Change Materials for Thermal Management in Lithium-Ion Battery Packs: A Review. Batteries, Journal, 11(12)(2025) 432.10.3390/batteries11120432.
32. Choi, H., H. Lee, U. Han, J. Jung, and H. Lee, Comparative Evaluation of Liquid Cooling-Based Battery Thermal Management Systems: Fin Cooling, PCM Cooling, and Intercell Cooling. International Journal of Energy Research 2024, 2024, 5395508.https://doi.org/10.1155/2024/5395508.
33. Dongellini, M., G. Martino, C. Naldi, S. Lorente, and G.L. Morini, Experimental study on the heat transfer performance of finned-tube heat exchangers in latent thermal energy storages: Effects of PCM types and operating conditions. Applied Thermal Engineering 2025, 271, 126273.https://doi.org/10.1016/j.applthermaleng.2025.126273.
34. Jayachandran, A., A.M. Kannan, and A. Basker, Passive thermal management of 21700 Li-ion batteries using plant-based eutectic phase change materials. International Journal of Heat and Mass Transfer 2026, 255, 127837.https://doi.org/10.1016/j.ijheatmasstransfer.2025.127837.
35. Zhao, Y., B. Zou, J. Ding, and Y. Ding, Experimental and numerical investigation of a hybrid battery thermal management system based on copper foam-paraffin composite phase change material and liquid cooling. Applied Thermal Engineering 2023, 218, 119312.https://doi.org/10.1016/j.applthermaleng.2022.119312.
36. Tong, L., X. Gong, S. Su, L. Xu, M. Liu, L. Chen, et al., Performance Improvement of a Honeycomb Battery Thermal Management System Based on Fin–Casing Synergistically Enhanced Heat Transfer. Batteries, Journal, 12(3)(2026) 94.10.3390/batteries12030094.
37. Balasubramanian, D., I.P. Venugopal, M. Subramanian, V. Raja, U. Kale, and J. Matijošius, Study on the battery thermal management system for cylindrical lithium-ion battery with nano-doped phase change material and liquid cooling. Scientific Reports 2025, 15, 24053.10.1038/s41598-025-08884-5.
38. Mane, Nikhil S., P. Kodancha, V. Hemadri, and S. Tripathi, Investigation on Cooling Performance of Composite PCM and Graphite Fin for Battery Thermal Management System of Electric Vehicles. Energy Storage 2024, 6, e70024.https://doi.org/10.1002/est2.70024.
39. Wang, C.-L. and J.C. Leong, Analysis of Thermal Management Strategies for 21700 Lithium-Ion Batteries Incorporating Phase Change Materials and Porous Copper Foam with Different Battery Orientations. Energies, Journal, 17(7)(2024) 1553.10.3390/en17071553.
40. Yang, H., M. Li, Z. Wang, and B. Ma, A compact and lightweight hybrid liquid cooling system coupling with Z-type cold plates and PCM composite for battery thermal management. Energy 2023, 263, 126026.https://doi.org/10.1016/j.energy.2022.126026.
41. Liao, G., W. Wang, F. Zhang, J. E, J. Chen, and E. Leng, Thermal performance of lithium-ion battery thermal management system based on nanofluid. Applied Thermal Engineering 2022, 216, 118997.https://doi.org/10.1016/j.applthermaleng.2022.118997.

 doi:10.20944/preprints202605.1153.v1

42. Jha, P., M. Hussain, and M.K. Khan, Numerical evaluation of nanofluid-based indirect liquid cooling of a Li-ion battery pack using equivalent circuit model under static and dynamic loading conditions. International Communications in Heat and Mass Transfer 2024, 159, 108079.https://doi.org/10.1016/j.icheatmasstransfer.2024.108079.
43. Wu, C., L. Wu, C. Qiu, J. Yang, X. Yuan, Y. Cai, et al., Experimental and numerical studies on lithium-ion battery heat generation behaviors. Energy Reports 2023, 9, 5064-74.https://doi.org/10.1016/j.egyr.2023.04.021.
44. Yousefi, E., D. Ramasamy, K. Kadirgama, V. Talele, H. Najafi, M. Olyaei, et al., Electrochemical-thermal modeling of phase change material battery thermal management systems: investigating mesh types for accurate simulations. International Journal of Heat and Mass Transfer 2025, 247, 127107.https://doi.org/10.1016/j.ijheatmasstransfer.2025.127107.
45. Zare, P., N. Perera, J. Lahr, and R. Hasan, A novel thermal management system for cylindrical lithium-ion batteries using internal-external fin-enhanced phase change material. Applied Thermal Engineering 2024, 238, 121985.https://doi.org/10.1016/j.applthermaleng.2023.121985.
46. Dai, Z., K. Nawaz, Y.G. Park, J. Bock, and A.M. Jacobi, Correcting and extending the Boomsma–Poulikakos effective thermal conductivity model for three-dimensional, fluid-saturated metal foams. International Communications in Heat and Mass Transfer 2010, 37, 575-80.https://doi.org/10.1016/j.icheatmasstransfer.2010.01.015.
47. Yang, H., Y. Li, Y. Yang, D. Chen, and Y. Zhu, Effective thermal conductivity of high porosity open-cell metal foams. International Journal of Heat and Mass Transfer 2020, 147, 118974.https://doi.org/10.1016/j.ijheatmasstransfer.2019.118974.
48. Liu, Q., F. Liu, S. Liu, Y. Wang, S. Panchal, M. Fowler, et al., Improved performance of Li-ion battery thermal management system by ternary hybrid nanofluid. Journal of Energy Storage 2025, 109, 115234.https://doi.org/10.1016/j.est.2024.115234.
49. Sun, W., P. Li, W. Cheng, C. Li, X. Qi, H. Shen, et al., Novel hybrid thermal management system for cylindrical lithium-ion battery based on CPCM and topology-optimized liquid cooling. Energy 2025, 329, 136719.https://doi.org/10.1016/j.energy.2025.136719.
50. Luo, D., L. Jiang, and Z. Wu, Enhanced thermal performance of a hybrid battery thermal management system with sandwich-structure phase change materials at a high discharge rate. Energy 2025, 324, 136032.https://doi.org/10.1016/j.energy.2025.136032.